Computational Modelling of Concrete and Concrete Structures – Meschke, Pichler & Rots (Eds)

Modeling inundation flooding in urban environments using density functional theory

E.D. Vartziotis, F.-J. Ulm & K. Boukin
Massachusetts Institute of Technology, Cambridge, MA, USA

R.J.-M. Pellenq
EpiDaPo Lab - CNRS / George Washington University, Children's National Medical Center, Children's Research Institute, Washington, DC, USA

Y. Magnin
Consultant, TotalEnergies, OneTech, Upstream R&D, CSTJF, Pau Cedex, France

K. Ioannidou
Laboratoire de Mécanique et Génie Civil, CNRS, Université de Montpellier, Montpellier, France

ABSTRACT: Evaluating the risk of inundation flooding and its deleterious effects in urban environments is key, considering that such natural disasters are poorly predictable, costly, and are expected to increase with global warming. To insight and evaluate flooding impact in cities and the role played by city textures, we propose a statistical physics computational approach called on-lattice density functional theory. Originally developed in Materials Science, the model is applied to the city scale, considered here as a porous media. We thus show that the strength of such an equilibrium-based approach stems from the combination of three aspects: *i.* the model has a minimum of inputs and an efficient computational time, *ii.* the model comes with an ease of modeling a variety of city elements that are critical for inundation flooding (*e.g.*, buildings, pavements, permeable soils, and drainage systems), *iii.* the model has physically meaningful output parameters, such as adsorption and desorption isotherms, which can be linked to a city's drainage capacity and steady-state gage heights. We found that isotherms exhibit a pronounced hysteresis, indicating that flooding and draining properties can be blocked in metastable microstates. Such behavior is key since it provides a fundamental means to qualitatively identify the risk of inundation flooding.

1 INTRODUCTION

Floods are one of the most common and costliest natural disasters in the United States and worldwide (FEMA 2021). Urban flooding is one of the greatest challenges to human safety, and it can cause severe damage to the economy and lead to high devastation (Tsubaki & Fujita 2010). The main factor that affects floodwater inundation and movement is the development of impervious surfaces, which do not allow natural drainage and inhibit infiltration of stormwater (Shuster et al. 2005). In addition to this, urban flooding may also occur due to non-mandatory building ordinances and non-consideration of the impact the city texture has. Specifically, the development of very dense building areas is prone to floods (National Academies of Sciences, Medicine, et al. 2019). Flood problems are expected to continue to rise and worsen due to climate change, as well as the expansion of cities and the increase of urban population (Pielke et al. 2002; Velasco et al. 2016). Studies have also shown that high atmospheric CO_2 concentrations lead to increased frequency of heavy daily precipitation events (Schreider et al. 2000). So, it is predicted that by 2100 the precipitation rates are expected to increase by 10–30% (Group 2021), and at the same time, the urban population is projected to increase from 55% to 68% by 2050 (UN 2018). These projections emphasize the importance of urban flood modeling and highlight the need for further development of existing flood models. In particular, they call for new reliable tools, that go beyond coarse grained empirical urban planning approaches based on mean land occupation density values (buildings, streets, drainage, green areas) (Özgen et al. 2016); empirical flood maps (FEMA 2018); and high-resolution empirical, hydrodynamic (2D shallow water equations (Teng et al. 2017)), and simplified conceptual models appropriate for building-project scale evaluation of flood inundation (Özgen et al. 2016). More specifically, to enhance the resilience of cities, there is a need to ascertain both a qualitative and quantitative link between city

DOI 10.1201/9781003316404-71

texture parameters, characteristic of the neighborhood scale in urban environment, and the risk of inundation flooding.

We approach this problem by means of a 'physics-by-analogy' simulation using on-lattice Density Functional Theory (DFT) (Kierlik et al. 2002; Zhou et al. 2019). This method, [1] was originally developed in statistical physics for pore-size characterization, gas adsorption-desorption, and capillary condensation phenomena in micro- and mesoporous materials (Lowell et al. 2006; Monfared et al. 2020; Rigby & Chigada 2009). In the DFT simulations, a virtual reservoir of particles is connected to the simulation box (here a portion of city as shown in Figure 1(a)), and particles are exchanged depending on the water particles chemical potential μ, which mimics the prescribed precipitation. This is being done to establish

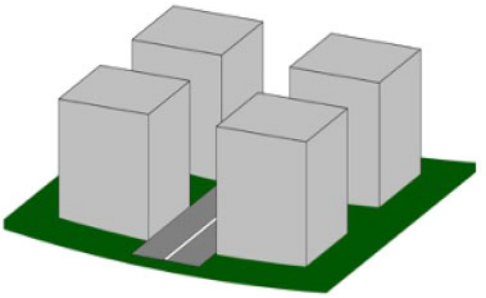

(a)

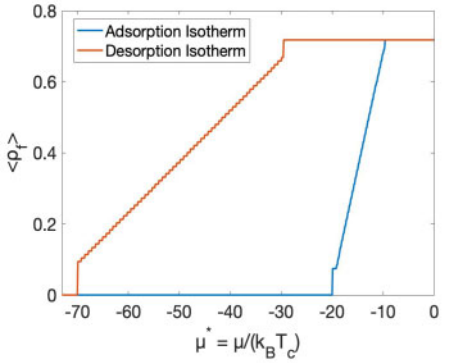

(b)

Figure 1. City model and isotherms. (a) Schematic of urban topography of side-length $L_x = L_y = 36$ m and height $H = 10$ m, consisting of buildings, and impermeable surface; (b) Adsorption - desorption density isotherms as a function of the dimensionless chemical potential, $\mu^* = \mu/(k_B T_c)$ and simulation parameters corresponding to: $a_{x,y}/a_z = 10$, $T^* = 0.8$, $\overline{w}^0_{sf} = 3$, $\overline{w}^0_{ff} = 6$.

[1] The DFT method herein employed should not be confused with the solid-state physics computational approach by the same name employed for electronic structure investigations of atoms and molecules (Roy 2019).

adsorption–desorption isotherms [Figure 1(b)], which can be used to qualitatively pin down the risk of inundation. The DFT-method hence minimizes the Grand potential [Eq.1], to determine the local equilibrium density on each lattice site i, with $\rho_i \in [0, 1]$ ($\rho = 0$ dry site, $\rho = 1$ water saturated site). In the system, each site interacts with its nearest neighbors (Kierlik et al. 2002), while those located at system edges interact through boundary periodic conditions. In addition, for the system we consider an unstructured lattice, allowing to locally increase the number of lattice sites, and so the accuracy of calculations in those regions. Thus, in this work, the lattice size in the elevation direction (z-direction) has been fixed smaller than the in-plane one in (x,y) directions.

2 METHODOLOGY

For a given urban configuration, the DFT method minimizes the dimensionless Grand potential, by adjusting iteratively the local densities $\rho_i \in [0, 1]$ (Kierlik et al. 2001):

$$\begin{aligned}\frac{\Omega}{k_B T_c} = \min_{\rho_i} \Bigg(& T^* \sum_i [\rho_i \ln \rho_i + (\eta_i - \rho_i) \ln (\eta_i - \rho_i)] \\ & - \sum_{<i,j>} (\overline{w}^i_{ff} \rho_i \rho_j + \overline{w}^i_{sf} [\rho_i (1 - \rho_j) + \rho_j (1 - \eta_i)]) \\ & - \mu^* \sum_i \rho_i \Bigg) \\ = & T^* \sum_i \eta_i \ln (1 - \frac{\rho_i}{\eta_i}) + \sum_{<i,j>} \overline{w}^i_{ff} \rho_i \rho_j \end{aligned} \tag{1}$$

where the local density of sites i read:

$$\rho_i = \eta_i [1 + \exp \left(- \frac{\overline{v}^{eff}_i}{T^*} \right)]^{-1}. \tag{2}$$

Here, η_i is the occupation number of site i; $T^* = T/T_c$ is the (kinetic) temperature, normalized by the critical temperature, T_c; $\mu^* = \mu/(k_B T_c)$ is the dimensionless chemical potential; $\overline{\omega}^i_{ff} = w_{ff}/(k_B T_c)$ and $\overline{\omega}^i_{sf} = w_{sf}/(k_B T_c)$ stand for dimensionless fluid-fluid and solid-fluid interaction parameters [in units of $k_B T_c$, with k_B the Boltzmann constant]; and $\overline{v}^{eff}_i$ stands for the dimensionless effective potential of site i,

$$\overline{v}^{eff}_i = \frac{v^{eff}_i}{k_B T_c} = \mu^* + \sum_{j/i} [\overline{w}^i_{ff} \rho_j + \overline{w}^i_{sf} (1 - \eta_j)]. \tag{3}$$

The sum over j is limited to the nearest neighbors of site i.

The Grand potential is minimized in a range of chemical potentials chosen to cover a full isotherm. To do so, we incrementally increase the chemical potential μ^* during the adsorption steps, from a large negative value, where no water adsorption occurs, up to a maximum value corresponding to the water saturation.

Once the adsorption phase is fully covered, we progressively decrease μ^* to simulate the desorption. For each subsequent value of $\mu_n^* = \mu_{n-1}^* \pm \Delta\mu^*$, we use the converged values of ρ_i at μ_{n-1}^* as initial condition for the next adsorption or desorption step (μ_n^*). For each μ^*, the convergence is considered to be reached when the density of two subsequent iterations is smaller than a threshold defined as, $(1/N)\sum_i(\rho_i^{(m+1)} - \rho_i^{(m)})^2 < 10^{-8}$ (Kierlik et al. 2002). Moreover, $\Delta\mu^*$ step sizes ranging from 10^{-1} to -10^{-3} have been chosen. The determination of isotherms, is finally obtained by averaging the full density as the sum of local densities as, $<\rho_f> = \frac{1}{N}\sum_i \rho_i$.

In the resulting isotherms, the water level or gage height, and the hysteresis loop qualitatively pin down the risk of inundation, and the city drainage efficiency, [Figure 1(b)] depending on the specific role played by city elements in the system. It is worth mentioning that for a linear filling process in a flat terrain, the average density $<\rho_f>$, coincides with the normalized gage height; whereas it is an integrated value of gage height distribution for complex terrains and city elements, that define the inundation risk of urban environments.

The entire system is composed of N lattice sites, occupied by either a fluid or a solid to delineate city elements (building, road, etc). This is defined by an occupation number η with fixed values 0 and 1, for solid and liquid sites, respectively. Hence, buildings are considered as repulsive surfaces with $\eta = 0$. Furthermore, $\eta = 0$ describes impermeable (*e.g.*, streets) surfaces; whereas permeable surfaces (*e.g.*, green areas) are identified by a mixture of occupation numbers of both ones and zeros, representative of the soil's porosity, $\phi = \overline{\eta}^{\text{soil}}$, where an overbar stands for averaging. Depending on the surface density of zero occupation numbers, we can identify soils with different porosities. Finally, water retention or the drainage system is identified as areas underground with $\eta = 1$, indicating sites where water can be stored before accumulating on the surface. Table 2 summarizes city elements with corresponding occupation numbers.

Table 1. Occupation number of city elements.

City elements	Occupation number η
Building	0
Street	0
Impermeable Soil	0
Permeable soil	0 & 1
Drainage System	1

One original addition to the DFT method for inundation modeling in urban environments is the elevation (z-direction) dependent fluid-fluid and solid-fluid interaction parameters, which were in the original model constant (Ioannidou et al. 2014; Pellenq et al. 2009). This allows us to consider the gravity-driven water filling process during precipitation. Thus, the z-direction dependency ensures a bottom-up filling during the adsorption process, and a top-down receding of the fluid phase during the desorption process. Following a constant hydrostatic gradient, we then use a linear relationship of the form:

$$\overline{w}_{kk}^i = \overline{w}_{kk}^0\left(1 - \frac{z_i - z_0}{\alpha_1 \cdot H_{ref}}\right); (kk = ff, sf), \tag{4}$$

where $1/(\alpha_1 \cdot H_{ref})$ defines the hydrostatic gradient, with α_1 a constant, and H_{ref} a reference height; z_i is the lattice site elevation; z_0 is the elevation of the lattice at the origin; and $\overline{w}_{kk}^0(kk = ff, sf)$ stand for reference values of the interaction parameters, with $\overline{\omega} = w_{sf}^0/w_{ff}^0$ in a dimensionless form. In the original DFT model, the interaction parameters ratio for water adsorption in cement has been reported as $w_{sf}/w_{ff} = 2.5$ (Bonnaud et al. 2012). However, such a parameter has been determined for capillary condensation in microscale structures, irrelevant at the city scale where such an effect is meaningless. For city modelization, dimensionless interaction parameters are city-specific, require a dedicated calibration, and will be discussed bellow. They need to be chosen with care in order to avoid occurrence of microscale phenomena that are irrelevant at city scale, such as capillary bridges (Zhou et al. 2019).

3 ISOTHERMS AS A MEANS TO ASSESS RISK OF INUNDATION FLOODING

To illustrate our purpose, we present below some features of the isotherms in section 3.1 in function of the most important DFT model parameters, and in section 3.2 for different drainage systems. As model system, we consider the city block displayed in Figure 1(a).

3.1 Influence of model parameters

To insight effects of DFT parameters on the water isotherm, we evaluate changes induced by the lattice sizes and their geometries, the effect of the temperature $T^* = T/T_c$, and the ratio of solid-fluid and fluid-fluid interactions, $\overline{\omega} = w_{sf}/w_{ff}$.

In Figure 2, we evidenced a negligible effect of the lattice sizes in the isotherm. A negligible effect is also found when varying the lattice geometry (keeping constant lattice sizes, $a_{x,y} = 0.5$ m and $a_{x,y} = 1$ m), from an isotropic case where $\alpha = a_{x,y}/a_z = 1$, to highly anisotropic ones, up to $\alpha = 100$. The lattice distortion, with a finer lattice discretization in the elevation direction, is found to be an important parameter affecting isotherm accuracy. More specifically, a fine enough elevation discretization reduces the size of finite jumps in the isotherms, while it does not modify the isotherm shape, value, or hysteresis loop. Thus, for determining relevant information about inundation gage heights, a fine enough elevation discretization is needed (typically, $a_z = 0.05$ m), whereas the in-plane discretization

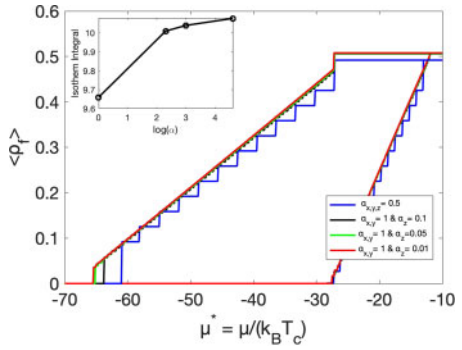

Figure 2. Impact of lattice size on isotherms: $a_{x,y,z} = 0.5$m (blue line), $a_{x,y} = 1$m and $a_z = 0.1$m (black line), $a_{x,y} = 1$m and $a_z = 0.05$m (green line), $a_{x,y} = 1$m and $a_z = 0.01$m (red line). The inset corresponds to the isotherm integral, plotted as the log of the lattice distortion α. Other simulation parameters correspond to $T^* = 0.8$, $\overline{\omega} = 0.5$.

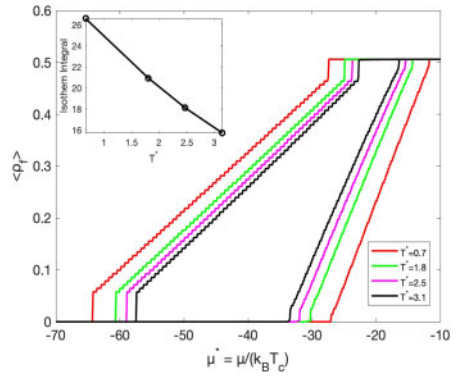

Figure 3. Impact of dimensionless temperature T^* on isotherms: $T^* = 0.7$ (red); $T^* = 1.8$ (green); $T^* = 2.5$ (pink); and $T^* = 3.1$ (black). The inset corresponds to the isotherm integral plotted vs. the dimensionless temperature T^*. Other simulation parameters correspond to $\alpha = 10$, $\overline{\omega} = 0.5$.

is fixed from the size of city elements (buildings, streets, green areas, etc.).

We now look at the effect of the temperature $T^* = T/T_c$ in isotherms. We recall that T^* is a dimensionless parameter, where the temperature T is normalized by the critical temperature T_c. In the simulations, we observe that values $T^* > 1$ entail a diffuse boundary between the gage height (water level) and the air, with density values ρ varying between 0 (gas) and 1 (liquid) over a finite thickness, whereas the (free) water boundary is demarcated for $T^* < 1$. This diffuse boundary for $T^* > 1$ affects the adsorption-desorption isotherms, both in size and absolute values, as shown in Figure 3.

In contrast to the overall role of T^* in the system's response, the fluid-fluid and solid-fluid interactions, or more specifically the interaction parameter ratio $\overline{\omega} = w_{sf}/w_{ff}$, play a prominent role in capturing the physics of adsorption and desorption of liquid into the city texture. This prominent role is shown in form of the adsorption-desorption isotherm in Figure 4 (a), and the snapshots shown in Figures. 4 (b) and (c) for two different values, $\overline{\omega} = 0.5$ and $\overline{\omega} = 5$. Figure 4 (a) shows that the onset of adsorption occurs at lower chemical potentials with increasing value of $\overline{\omega}$; and the same shift occurs at the end of the desorption process. This shift is due to the increase in the solid-fluid interaction, which favors the adsorption of water onto surfaces leading eventually to menisci formation [compare Figures. 4 (b) and (c)]. Such menisci are highly relevant for wetting phenomena at nano- and mesoscale of porous materials, but they do not represent the physics of inundation at the city scale, and need to be avoided.

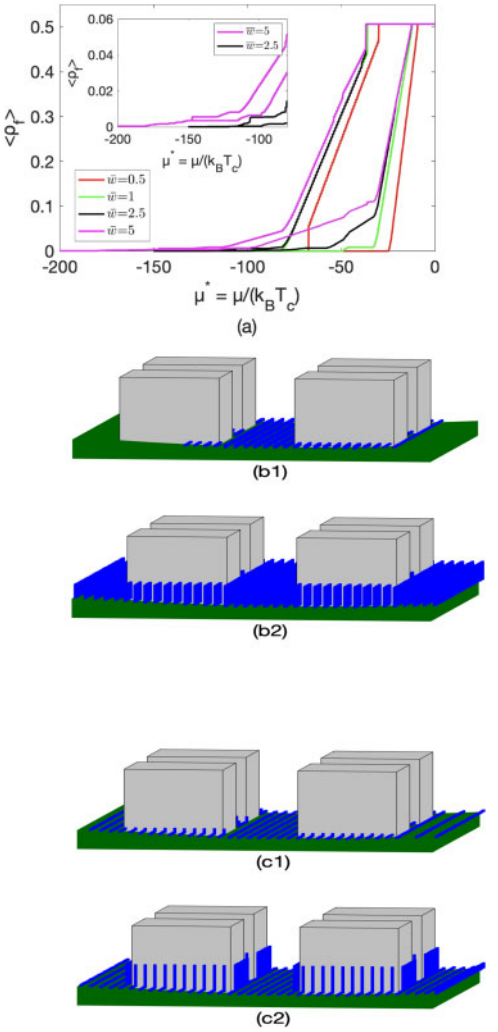

Figure 4. (a) Impact of interaction parameter ratio $\overline{\omega} = w_{sf}/w_{ff}$ on isotherms: $\overline{\omega} = 0.5$ (red line); $\overline{\omega} = 1$ (green line); $\overline{\omega} = 2.5$ (black line); $\overline{\omega} = 5$ (pink line). (b1-c2) Snapshots of surface filling for different values of $\overline{\omega}$ and chemical potential μ^*: (b1) $\overline{\omega} = 0.5$ & $\mu^* = -24$; (b2) $\overline{\omega} = 0.5$ & $\mu^* = -19$; (c1) $\overline{\omega} = 5$ & $\mu^* = -98$; (c2) $\overline{\omega} = 5$ & $\mu^* = -69$. Other simulation parameters correspond to $\alpha = 10$, $T^* = 0.8$.

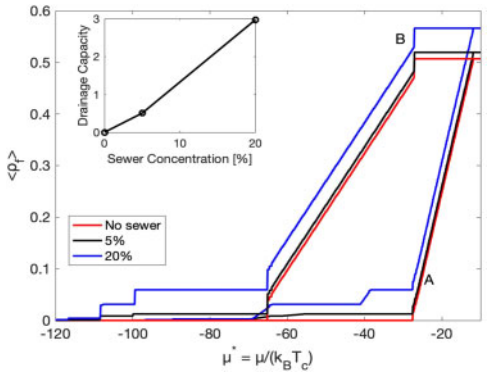

Figure 5. Impact of the city's drainage system on isotherms: No sewer (red line); 5% sewer (black line); 20% drainage (blue line); the inset corresponds to the area of hysteresis loop for the adsorption - desorption loop of the sewer vs. sewer concentration. Other simulation parameters correspond to $\alpha = 10$, $T^* = 0.8$.

3.2 *Impact of drainage and soil porosity on risk of inundation flooding*

Inundation flooding of urban environments results from the imbalance between precipitation and drainage. While precipitation is incorporated in the DFT approach by the chemical potential, μ^*, drainage in our DFT approach is captured in form of either a pipe system or a distributed soil drainage system, considering a spatial distribution of the occupation number in the soil (see Table 2). We compare the impact of pipe and soil drainage on isotherms.

Simulations are carried out for three drainage system concentrations, 0, 5, and 20% representative of the volume fraction of the underground where water can accumulate. The adsorption-desorption isotherms for the three systems are shown in Figure 5. These isotherms are characterized by a change in slope, from the almost horizontal branch during pipe drainage, followed by an almost vertical branch once the pipes are filled. The necking point, $< \rho_f >_d$, between these two regimes [denoted by (A) in Figure (5)] increases with the drainage concentration, from $< \rho_f >_d = 0$ for the system without drainage, to $< \rho_f >_d = 0.06$ for the 20%-drainage system. This density shift is constant over the entire adsorption-desorption isotherm [point (B) in Figure (5)], and can thus be considered as a qualitative measure of the impact of drainage at the scale of the simulated city block. If one considers an adsorption-desorption loop to the chemical potential μ_d at the necking point, the area below the curve can be viewed as a measure of building block's drainage capacity [see inset of Figure 5]. This means that the effective gage height above ground is reduced by this drainage (water storage) capacity.

Similar drainage capacity measures are obtained when considering a permeable soil, i.e. a soil which can retain water in our equilibrium-based approach. Such a soil is modeled in the DFT approach through an occupation number distribution in the soil, with a porosity of $\phi = \overline{\eta}^{\text{soil}}$ and surface solid-fluid interactions, $\omega = 1$. A comparison for three different porosity values, $\phi = 0, 25, 50\%$, is shown in Figure 6 in terms of the adsorption-desorption isotherms. Similar to pipe drainage [Figure 5], a porous soil entails a vertical shift of the isotherms, defined by a necking point. However, the drainage capacity calculated from the integral over the adsorption-desorption hysteresis loop [inset of Figure 6], exhibits smaller values when compared to pipe drainage [inset of Figure 5]. This observation can be attributed to the distributed nature of the porosity in the ground when compared to the concentrated nature of drainage pipes. While difference in different drainage systems merits further investigation, it shows the potential of the DFT approach to qualitatively discern the role of city-scale drainage systems in inundation flooding.

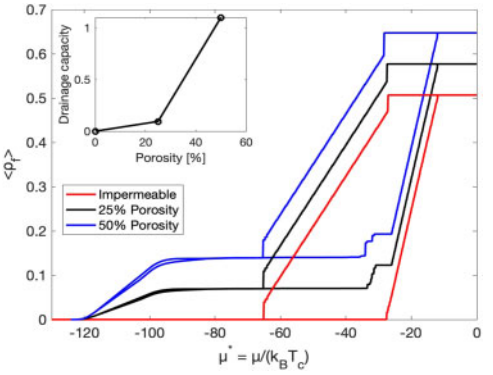

Figure 6. Impact of the soil's permeability on isotherms: Impermeable soil $\phi = 0\%$ (red line); permeability $\phi = 25\%$ (black line); permeability $\phi = 50\%$ (blue line); the inset corresponds to the area of hysteresis loop for the adsorption - desorption loop of the soil vs. soil porosity. Other simulation parameters correspond to $\alpha = 10$, $T^* = 0.8$.

4 CALIBRATION

This on-lattice DFT approach requires calibration of the α_1 and the $\overline{w}^0_{kk}$ parameters of the interaction parameters, and the chemical potential μ^*, to gain quantitative capabilities for urban flood risk evaluation. For that purpose, we use an optimization algorithm, the genetic algorithm (GA) (MathWorks 2021), and a reference model developed by the MIT Office of Sustainability (MITOS), against which we calibrate the model parameters. MITOS is using the InfoWorks ICM (Integrated Catchment Modelling) model (Innovyze 2021), a software platform for integrated 1D /2D hydrodynamic modeling (Ltd 2021). The applied optimization algorithm finds the best fit for the three model parameters by minimizing the mean of the height difference between the DFT model and the reference predictions:

$$fl = \min_{\alpha_1, \overline{w}^0_{kk}, \mu^*} \left(mean\left[ICM_{Height} - DFT_{Height} \right]^2 \right), \qquad (5)$$

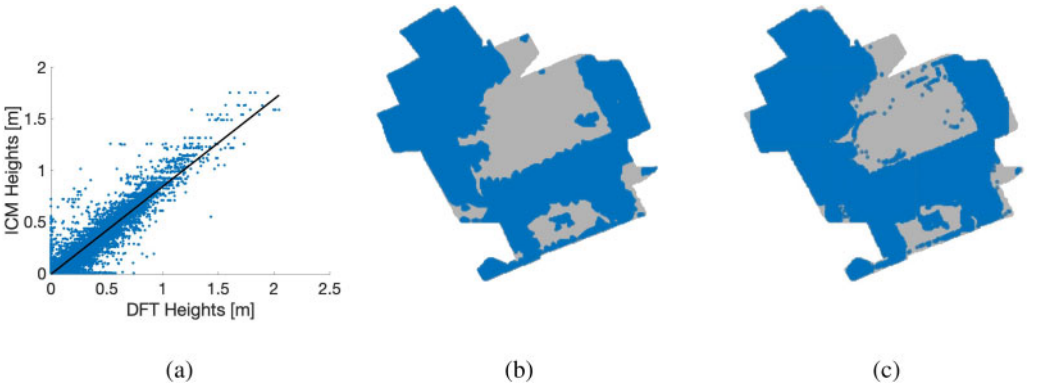

Figure 7. Results for Danforth St. sub-catchment for the 100 year storm event under current climate conditions (a) ICM vs. DFT height values; water distribution for (b) the ICM model; (c) the DFT model at $\mu^* = -0.577$.

where fl is the minimized function; ICM_{Height} are the flood heights obtained by the ICM model for six precipitation events (see Table 5); and DFT_{Height} are the equivalent flood heights obtained by the DFT model.

For the model calibration, we have chosen as our study area the MIT campus, and more specifically, the sub-catchment on Danforth Street. This sub-catchment is considered for the calibration with impermeable surfaces and no city elements. In Table 5 we see the results after the calibration for the average flood heights for the ICM and the DFT model and the corresponding chemical potential μ^*. The quality of the calibration is illustrated by comparing the ICM and DFT height values for the same (x,y) points. Figure 7 (a) displays the spread of height values obtained from the two models for the 100-year storm event under current climate conditions in the form of a cross plot. The R^2-value for the simulation is 0.9154 showing a close to linear correlation. The corresponding water distribution on the sub-catchment for the 100-year precipitation event, shown in Figure 7 (b) and (c), indicate that both models are mainly flooding the same areas. The correctness of this distribution must be further studied and validated.

5 DISCUSSION

The proposed DFT-model for inundation flooding departs from the premise that an equilibrium-based model built around the minimization of the Grand potential [i.e., Eq. (1)] can capture essential features of the physics of inundation of urban environments. It is thus of interest to test this conjecture by comparing the DFT approach with the most common approach for inundation modeling, which is based upon the shallow-water equations (SWE). The SWE-model condenses the laws of mass and momentum conservation into a continuum 2D-boundary layer in between terrain height $b(x,y)$ and free surface height $b+h$, considering the in-plane flow velocity vector $\vec{u}(x,y,t) = (u,v)$. Mass conservation reads (Vreugdenhil 1994):

$$\frac{\partial h}{\partial t} + \nabla \cdot (h\vec{u}) = p_z - d_z, \tag{6}$$

and momentum conservation:

$$\frac{\partial (h\vec{u})}{\partial t} + \nabla \cdot (h\vec{u} \otimes \vec{u}) = -gh\nabla(b+h), \tag{7}$$

where p_z is the precipitation rate; d_z the drainage rate; g the earth acceleration, b the terrain height (measured e.g. w.r.t. seal level). The underlying assumptions of the SWE-model are (Teng et al. 2017; Vreugdenhil 1994): (1) horizontal variations in velocity are much greater than vertical variations, so that the velocity $\vec{u}(x,y,t)$ can be viewed as depth-averaged in-plane velocities; (2) vertical accelerations can be neglected (boundary layer assumption); and (3) the pressure gradient over the height is negligible compared to in-plane pressure gradients. The focus of this discussion is to identify commonalities and differences with the proposed DFT approach.

The first point in common is the outcome of both approaches, namely spatially resolved flood height estimates, coined gage height in the case of classical approaches (Ali et al. 2016), and adsorption-desorption isotherms in the DFT approach. In the SWE approach, this gage height at a point (x,y) is attained once mass and momentum conservation has balanced in time the imbalance between precipitation and drainage rate. In the DFT approach the system is put in contact with an (outside) virtual bath of particles at a chemical potential μ, and so in first order, the precipitation rate, p_z, can be captured by a Newton-type kinetics law of the form $p_z \sim \frac{\mu_0^* - \mu^*}{k_p}$, with k_p an exchange coefficient. Similarly, it is tempting to formulate the drainage rate in terms of DFT modeling

quantities. For instance, for drainage by a permeable soil, the drainage rate, d_z, is driven by the soil saturation rate S, meaning $d_z \sim \frac{dS}{dt}$, where $S \sim \frac{\overline{\eta\rho}^{\text{soil}}}{\overline{\eta}^{\text{soil}}}$.

Herein, $\overline{\eta}^{\text{soil}}$ is the soil porosity, whereas $\overline{\eta\rho}^{\text{soil}}$ is the part of this porosity saturated by the fluid phase. The determination of the drainage rate in the SWE model thus requires additional information about water retention in order to become operational (Massari et al. 2014). In contrast, in the DFT model, the soil and its water retention capacity are explicitly included in the minimization of the Grand potential [see Eq. 1 and Table 2].

Table 2. Calibration results for Danforth Street.

Storm	ICM Height	μ^*	DFT Height
10Y 24H today	0.1255	–0.5824	0.1235
10Y 24H 2030	0.1439	–0.58	0.1789
10Y 24H 2070	0.163	–0.5789	0.2121
100Y 24H today	0.2267	–0.577	0.2444
100Y 24H 2030	0.2598	–0.5743	0.2783
100Y 24H 2070	0.2982	–0.571	0.3148

In the equilibrium-based DFT approach, all relations are time-independent. It excludes flash flood phenomena (Vreugdenhil 1994), the complex interplay between soil saturation and drainage (Teng et al. 2017), and the non-stationarity of gage height distribution in urban environments (Group 2021). In return, it can be viewed as an asymptotic state of inundation flooding for urban environments, and hence an appropriate means for a first-order evaluation of the risk of inundation flooding. Finally, it should be noted that the assumption of stationarity does not necessary imply a zero-flow velocity. It only means that the first term on the l.h.s. of respectively Eq. (6) and Eq. (7) is zero, but not the second one.

6 CONCLUSIONS AND PERSPECTIVES

The method herein proposed provides a simulation-based adsorption technique dedicated to urban environments at the city scale. To the best of our knowledge, such an approach is original in its attempt to transpose by analogy the physics of coarse-grain adsorption techniques commonly employed in Materials Science to city scale. While the equilibrium-based approach discards the time-dependence of flooding, the strength of the DFT method stems from a combination of a minimum of input quantities, the ease of modeling city elements (buildings, pavements, drainage systems, soil saturation, etc.), and physically meaningful output parameters which can be linked to a city's drainage capacity, risk of inundation flooding and so on. A further strength of the approach is the well-posed and computationally efficient minimization problem.

While the results so far obtained illustrate the potential to qualitatively capture inundation features in an urban environment, there are several steps required for the approach to gain quantitative capabilities for risk evaluation. This includes (1) the further development of the calibration by adding more elements into the calibration, such as permeable soils, drainage systems, etc.; (2) the water distribution validation via the so-called two-point correlation function; (3) the systematic investigation of the role of city texture parameters; and (4) based on a clear understanding of the governing city texture parameters, it should be possible to identify means of mitigating the impact of inundation flooding. It is expected that the proposed approach will contribute to the emerging field of 'urban physics' (Sobstyl et al. 2018).

7 ACKNOWLEDGEMENT

This research was carried out by the Concrete Sustainability Hub (CSHub@MIT), with funding provided by the Portland Cement Association (PCA) and the Ready Mixed Concrete Research & Education Foundation (RMC EF). The CSHub@ MIT is solely responsible for content. Additional support was provided by the MIT Office of Sustainability (MITOS@MIT).

REFERENCES

Ali, H., P.-Y. Lagrée, & J.-M. Fullana (2016). Application of the shallow water equations to real flooding case.

Bonnaud, P., Q. Ji, B. Coasne, R.-M. Pellenq, & K. Van Vliet (2012). Thermodynamics of water confined in porous calcium-silicate-hydrates. *Langmuir 28*(31), 11422–11432.

FEMA, F. E. M. A. (2018). Guidance for Flood Risk Analysis and Mapping - Flood Risk Assessments. https://www.fema.gov/sites/default/files/2020-02/Flood_Risk_Assessment_Guidance_Feb_2018.pd. [Online; accessed January-2021].

FEMA, F. E. M. A. (2021). Floods. https://www.ready.gov/floods. [Online; accessed June-2021].

Group, W. B. (2021). Climate Change Knowledge Portal, Laos County Historical Climateb Data. https://climateknowledgeportal.worldbank.org/country/laos/climate-data-projections. [Online; accessed January-2021].

Innovyze (2021). ICM. https://www.innovyze.com/en-us/products/infoworks-icm. [Online; accessed June-2021].

Ioannidou, K., R. J.-M. Pellenq, & E. Del Gado (2014). Controlling local packing and growth in calcium–silicate–hydrate gels. *Soft Matter* 10(8), 1121–1133.

Kierlik, E., P. Monson, M. Rosinberg, & G. Tarjus (2002). Adsorption hysteresis and capillary condensation in disordered porous solids: a density functional study. *Journal of Physics: Condensed Matter 14*(40), 9295.

Kierlik, E., M. Rosinberg, G. Tarjus, & P. Viot (2001). Equilibrium and out-of-equilibrium (hysteretic) behavior of fluids in disordered porous materials: Theoretical predictions. *Physical Chemistry Chemical Physics 3*(7), 1201–1206.

Lowell, S., J. E. Shields, M. A. Thomas, & M. Thommes (2006). Characterization of porous solids and powders: surface area, pore size and density. *16*.

Ltd, A. (2021). InfoWorks ICM – The Most Powerful 1D/2D Integrated Catchment Modeling Solution. https://www.aquamod.eu/en/index.php/software/infoworks-icm?showall=1. [Online; accessed June-2021].

Massari, C., L. Brocca, T. Moramarco, Y. Tramblay, & J.-F. D. Lescot (2014). Potential of soil moisture observations in flood modelling: Estimating initial conditions and correcting rainfall. *Advances in Water Resources 74*, 44–53.

MathWorks (2021). What Is the Genetic Algorithm? https://www.mathworks.com/help/gads/what-is - the - genetic - algorithm.html. [Online; accessed July-2021].

Monfared, S., T. Zhou, J. E. Andrade, K. Ioannidou, F. Radjaï, F.-J. Ulm, & R. J.-M. Pellenq (2020). Effect of confinement on capillary phase transition in granular aggregates. *Physical Review Letters 125*(25), 255501.

National Academies of Sciences, E., Medicine, et al. (2019). Framing the challenge of urban flooding in the united states.

Özgen, I., J. Zhao, D. Liang, & R. Hinkelmann (2016). Urban flood modeling using shallow water equations with depth-dependent anisotropic porosity. *Journal of Hydrology 541*, 1165–1184.

Pellenq, R. J.-M., A. Kushima, R. Shahsavari, K. J. Van Vliet, M. J. Buehler, S. Yip, & F.-J. Ulm (2009). A realistic molecular model of cement hydrates. Proceedings of the National Academy of Sciences 106(38), 16102–16107.

Pielke, R. A., M. W. Downton, & J. B. Miller (2002). Flood damage in the united states, 1926-2000: a reanalysis of national weather service estimates.

Rigby, S. P. & P. I. Chigada (2009). Interpretation of integrated gas sorption and mercury porosimetry studies of adsorption in disordered networks using mean-field dft. *Adsorption 15*(1), 31–41.

Roy, A. K. (2019). A new density functional method for electronic structure calculation of atoms and molecules. *arXiv preprint arXiv:1904.08806*.

Schreider, S. Y., D. Smith, & A. Jakeman (2000). Climate change impacts on urban flooding. *Climatic Change 47*(1), 91–115.

Shuster, W. D., J. Bonta, H. Thurston, E. Warnemuende, & D. Smith (2005). Impacts of impervious surface on watershed hydrology: A review. *Urban Water Journal 2*(4), 263–275.

Sobstyl, J., T. Emig, M. A. Qomi, F.-J. Ulm, & R.-M. Pellenq (2018). Role of city texture in urban heat islands at nighttime. *Physical review letters 120*(10), 108701.

Teng, J., A. J. Jakeman, J. Vaze, B. F. Croke, D. Dutta, & S. Kim (2017). Flood inundation modelling: A review of methods, recent advances and uncertainty analysis. *Environmental modelling & software 90*, 201–216.

Tsubaki, R. & I. Fujita (2010). Unstructured grid generation using lidar data for urban flood inundation modelling. *Hydrological Processes: An International Journal 24*(11), 1404–1420.

UN (2018). 2018 Revision of World Urbanization Prospects Web-based resource (New York: The Population Division of the Department of Economic and Social Affairs of the United Nations). https://www.un.org/development/desa/publications / 2018 - revision - of - world - urbanization - prospects.html. [Online; accessed January-2021].

Velasco, M., À. Cabello, & B. Russo (2016). Flood damage assessment in urban areas. application to the raval district of barcelona using synthetic depth damage curves. *Urban Water Journal 13*(4), 426–440.

Vreugdenhil, C. B. (1994). Numerical methods for shallow-water flow. *13*.

Zhou, T., K. Ioannidou, E. Masoero, M. Mirzadeh, R. J.-M. Pellenq, & M. Z. Bazant (2019). Capillary stress and structural relaxation in moist granular materials. *Langmuir 35*(12), 4397–4402.

Zhou, T., K. Ioannidou, F.-J. Ulm, M. Z. Bazant, & R.-M. Pellenq (2019). Multiscale poromechanics of wet cement paste. *Proceedings of the National Academy of Sciences 116*(22), 10652–10657.